An Algorithm for Rapid Adjustment of Lower Extremity Posture of a Pedestrian Model

Jisi TANG[1,2], Jingwen HU[2], Bingbing NIE[1], Qing ZHOU[1]

1. State Key Laboratory of Automotive Safety and Energy, Department of Automotive Engineering, Tsinghua University, Beijing, China
2. University of Michigan Transportation Research Institute, Ann Arbor, MI, USA

Abstract

Posture adjustment of finite element (FE) human body model is a significant step in accident reconstruction and investigation on pedestrian kinematical and injury outcomes. A rapid posture adjustment algorithm for pedestrian lower extremities was developed to account for realistic joint kinematics during a gait cycle. Under the kinematic constraints from joint anatomy, the algorithm calculated the posture of the lower extremity at any instant of a gait cycle from the open kinematic chain linked by the hip, knee and ankle joints in sequence. Joint motions were predicted based on subject-specific geometry, following the rules of joint motion based on the literature. Mesh morphing method were implemented to calculate nodal coordinates of soft tissues around the joints.

As an application example, the proposed algorithm was exercised on the midsize male GHBMC pedestrian model and three different walking postures within a gait cycle were generated. These models were used to simulate a typical vehicle-to-pedestrian crash scenario. Pre-crash posture showed significant effect on the injury risks of lower extremities, indicating necessity of taking pre-crash postures into account for pedestrian injury investigation.

Keywords Finite element human body model, pre-crash posture, posture adjustment, subject-specific geometry, mesh morphing

I. INTRODUCTION

Fatalities of pedestrian in road traffic accidents have become a world-wide public health problem. Each year over 1.2 million people die and 20–50 million people are injured in motor-vehicle crashes around the world, and pedestrians account for more than a third of them [1]. The pedestrian kinematics and injuries in vehicle collisions are influenced by vehicle velocity, type of vehicle, stiffness and shape of the vehicle front, anthropometry of the pedestrian, as well as the initial posture and kinematics of the pedestrian relative to the vehicle front [2]. The Pedestrian Crash Data Study (PCDS) from the US showed that 55% of pedestrians were walking prior to the crash [3]. A study in the EU 5th Framework Project HUMOS2 with 1671 cases showed that 79% of the pedestrians were in motion rather than staying still [4]. Studies from Elliott et al. [5] and Peng et al. [6] pointed out that pedestrian head impact conditions would be influenced by pedestrian gait. Untaroiu et al. proposed a way to identify pedestrian posture prior to impact with optimization method in vehicle-to-pedestrian impact accident reconstruction [7]. Studies from Elliott and Untaroiu were conducted with multi-body human model in MADYMO. Li et al. utilized finite element (FE) human body model adjusted to different stances and did a preliminary investigation on the influence of pedestrian gaits on kinematics and injury outcomes of lower extremities [8]. Tang et al. compared the kinematics between standing and walking based on simulations with THUMS pedestrian model [9]. In general, walking posture presented higher risk in soft tissue failure and in contrast lower risk in bone fracture under lateral impact. To fully investigate the injury mechanisms behind different postures, the most intuitive method is to do cadaveric tests with subjects adjusted to target postures. Due to the diversity of the specimens, results of the experiments are sometimes not comparable. Test surrogates could help to improve repeatability of the experiments, such as physical dummies,

Jisi Tang is a Ph.D. student, Bingbing Nie is assistant Professor and Qing Zhou is Professor in the Department of automotive engineering at Tsinghua University in China (Phone: +86-10-62789421, Email: zhouqing@tsinghua.edu.cn). Jingwen Hu is Associate Research Scientist in University of Michigan Transportation Research Institute in US.

whose joints are hinges enabling adjacent parts to rotate relative to each other to change pre-crash posture. Corresponding virtual dummies are also posture adjustable with joint definition either in MADYMO or FE environment. For FE human body model, conventional method to do posture adjustment is by pre-simulation, which is typically associated with high computational cost and insufficient accuracy of realistic walking motion. Comparing to the method for posture adjustment implemented in dummy and multi-body model, a hypothesis emerges. That is, whether FE human body model could be adjusted to target posture directly with rotation and/or translation at joint area, instead of conducting simulation with applying quasi-static load, and will this adjustment be accurate enough in anatomical view. Jani et al. had developed a graphics-based method to reposition knee joint of FE human body model with bone repositioned based on averaging experimental data and skin parts being calculated by geometric heuristics [10]. In this study, prediction of flexion-extension motion was processed based on instant center determined by statistical test results, leading to potential discrepancy of joint motion due to subject-specific geometry deviating from averaged experimental data.

The objective of this study is to develop an efficient algorithm for rapid adjustment of pedestrian model postures within a full gait cycle considering realistic human joint kinematics. Joint motion reconstruction was performed based on subject-specific geometry. And mesh morphing method was adopted to calculate deformation of transitional soft tissues, i.e., ligaments and flesh. The developed algorithm was exercised based on 50th percentile male GHBMC pedestrian model. Three pedestrian models with different walking postures within a gait cycle, i.e., heel contact, toe off and mid-swing stances, were generated. These models were used to simulate a 30 kph vehicle-to-pedestrian crash scenario and the predicted injury outcomes were analyzed.

II. METHODS

Method overview

To adjust FE human model to a target posture, under the kinematic constraints from joint anatomy, the proposed algorithm calculated the posture of the lower extremities from the open kinematic chain linked by the hip, knee and ankle joints in sequence (Figure 1). To accurately define the instant posture and joint motion of pedestrian lower extremities, we referenced the terms which are widely used in the field of gait analysis. For walking posture, angle history curves for each joint from 0 to 100 percent gait status were established [11]. At any instant, angle for each joint in lower extremity can be determined.

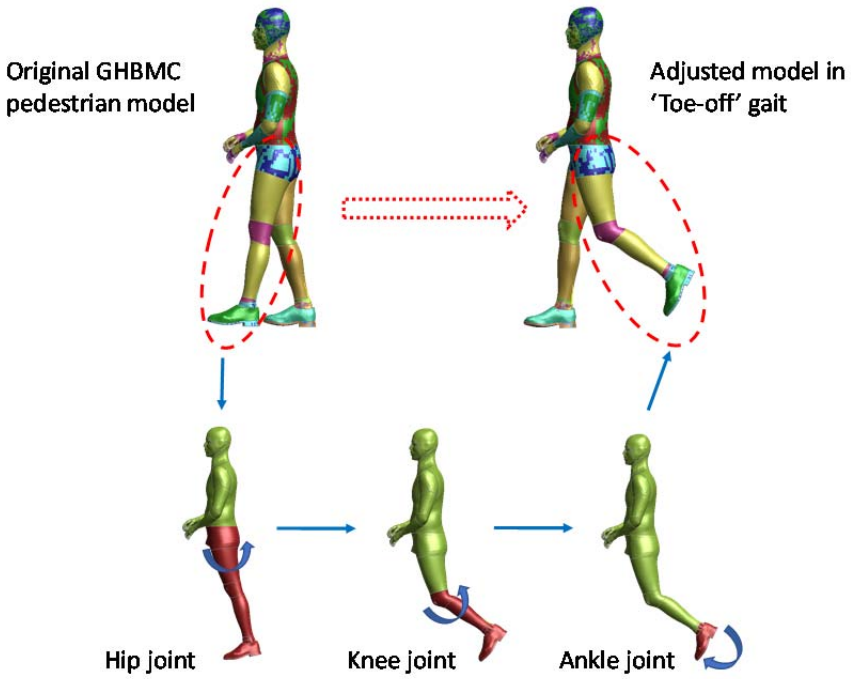

Fig. 1. Schematic of posture adjustment process. In the figure original GHBMC pedestrian model was adjusted to 'toe-off' gait. For left leg, joint motion was calculated in an open kinematic chain of hip, knee and ankle joint in sequence.

Joint motion was analyzed to determine relative motion of bone structures in each articulation. Based on literatures, knee joints approximately exhibited 2 degrees-of-freedom spatial motions; hip joints were treated as a spherical hinge at the geometrical center of femur head. In vehicle-to-pedestrian impact, initial contact was commonly around knee joints and tibia shaft area. Thus, ankle joints were of lower injury risks relative to other joints. In this study, ankle joints were simplified as spherical joints to globally match the target posture.

During reposition of each joint, relevant components of the human model were divided into three categories, i.e., static, moving and transitional. Joint motion was depicted as moving parts being driven by active muscles to move around the static parts. Coordinates of nodes in moving parts were calculated numerically to represent reposition of joint motion, with coordinates of nodes in static parts being unchanged. Soft tissues, such as ligaments and flesh around the joint, deformed with skeleton motion, whose nodal coordinates were calculated by interpolation using a mesh morphing method. Taking knee joint as an example, the tibia and adjacent components ('moving parts') were rotated along the axis connecting instant centers of curvature on medial and lateral femoral condyles ('static parts'). Here, "instant center of curvature" corresponded to local curvature of intersecting line generated by cut plane at the contact point, differing from "instant center" in motion analysis of rigid body. Soft tissues around the joints were treated as 'transitional component' (Figure 2).

The proposed algorithm was exercised based on 50th percentile male GHBMC pedestrian model. Three pedestrian models with different walking postures within a gait cycle, i.e., heel contact, toe off and mid-swing stances, were generated. These models were used to simulate a 30 kph vehicle-to-pedestrian crash scenario and predicted injury outcomes were analyzed.

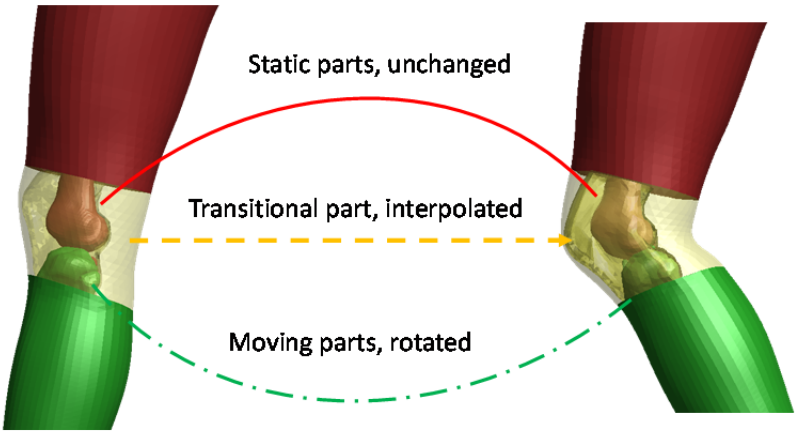

Fig. 2. Illustration of categorization of static, moving and transitional parts in reposition of knee joint

Algorithm for determining joint motions

Determination of moving part motion was conducted based on analysis of realistic joint kinematics. Hip joint was defined as a spherical joint, where the outer surface of acetabulum and femur head were approximated as spherical surfaces. Rotation of the femur and attached parts was conducted along the axis passing through center of femur head. Matrix for calculation of the relevant parts is provided in Appendix A. Calculation of the ankle joint motion was similar, and the rotation center was placed at the middle point between the medial and lateral malleolus centers.

Knee joint exhibited complicated spatial motion between adjacent femur and tibia. Taken femur as reference, motion of tibia and attached components are of six degrees of freedom (DOFs) from perspective of orthopedics - flexion/extension, adduction/abduction, internal/external rotation, anterior/posterior translation, superior/inferior translation and medial/lateral translation [12].

The two joint interfaces – medial and lateral joint interface between femoral condyles and tibial plateau would sustain compression loading and maintain in contact during normal gait given the fact that cartilages at knee joints were loaded continuously in a full gait cycle [13]. From a kinematical view of the joint motion, the two interfaces were taken as two constrain faces, with each constraining one global DOF in the dynamic system. The two DOFs were corresponding to superior/inferior translation and adduction/abduction of tibia. Experimental studies and simulation results both pointed out that displacement of medial/lateral and anterior/posterior translation was less than 2 mm at most time within a full gait cycle [14][15]. Thus motions in

such DOFs were not taken into account given their insignificant motion.

Referring to D'Alembert's principle, knee joint motion could be simplified as a two degree-of-freedom motion in space – flexion/extension, and internal/external rotation. Flexion/extension is the dominant knee joint motion during walking. To decouple the two motions, the axis of flexion was calculated while maintaining the contact point on the tibial plateau. The axis of flexion was calculated as the line connecting "instant centers of curvature" on the two femoral condyles. This guaranteed that tibia presented pure sliding along femoral condylar surfaces, i.e., at any instant the contact points would be relatively static on the tibial plateau. Such definition was consistent with approach to describe flexion in previous study [16].

To accurately calculate the instant center of the local curvature of intersecting line generated by cut plane at the contact point, and axis of flexion at any instant gait cycle, several steps were carried out as following.

1. Determination of contact points
2. Calculation of local curvature at contact point
3. Generation of instant center of curvatures and axis of flexion

The first step was to determine the contact points at medial and lateral interface between femoral condyle and tibial plateau, as point A and B in Figure 3. The surfaces were discretized into pieces of shell elements in FE model, implying that coordinates of contact points cannot be explicitly extracted from the model. Surfaces at the vicinity of the contact points needed to be expressed in analytical form for calculation of the coordinates. Lagrangian interpolation method were implemented to generate analytical expression of the local surface around contact points. Detailed formulations were provided in Appendix B.

Take point B, the contact point for lateral femoral condyle as an example (Figure 4). On the surface reconstructed around point B, each point was associated with its own tangent and normal vectors. To calculate tangent vectors of local surface, covariant derivatives were specified at the point. Two tangent vectors were generated since surface was 2-dimensional. Normal vector was cross production of the tangent vectors, as shown in Figure 4. Coordinates of contact point could be determined based on the criterion that normal vector of contact point should be parallel with normal vector of tibial plateau, where tibial plateau was approximated as a plane (Figure 3).

When coordinate of B had been determined as $\boldsymbol{X}_B$, coordinate of point D could be expressed as (1) in Figure 4, indicating that the instant center of curvature was the contact point shifted by a distance R (instant radius) along normal vector.

$$\boldsymbol{X}_D = \boldsymbol{X}_B + R\boldsymbol{n}, \tag{1}$$

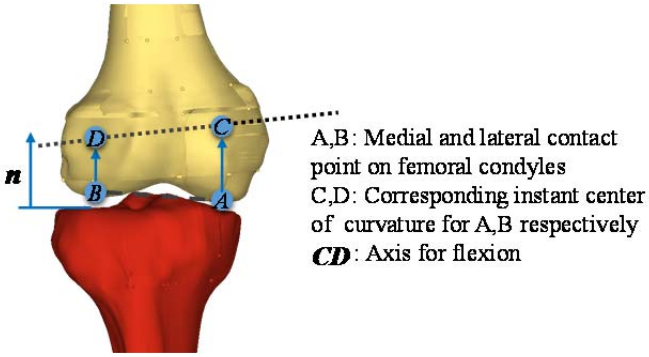

Fig. 3. Illustration of location of contact points (point A and B) and definition of axis of flexion (vector CD connecting the instant centers of curvature for medial and lateral femoral condyles respectively)

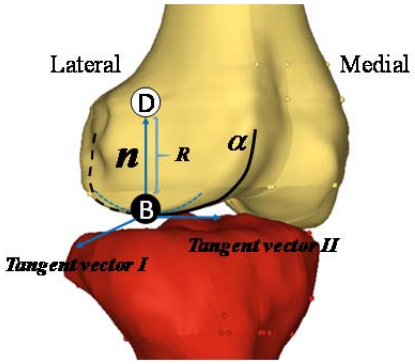

Fig. 4. Schematic of determination of contact point B, instant center of curvature of curvature D, normal vector ***n***, and instant radius at lateral femoral condyle

To calculate the instant radius, or curvature of curve at a specific point towards a given direction, method introduced by differential geometry was implemented. Such method calculated above mentioned local curvature by (2).

$$\kappa = -\frac{II}{I}, \tag{2}$$

κ was the curvature at point B. I and II were the first and second fundamental forms of a surface Introduction to calculation of tangent vectors, normal vector, I and II was given in Appendix C. Distance between the contact point B and instant center of curvature D, abbreviated as R indicating length of the vector $\boldsymbol{BD}$, was the reciprocal of curvature κ.

$$R = |\boldsymbol{BD}| = \frac{1}{\kappa}, \tag{3}$$

Similar method was carried out on determination of coordinates of point C. Axis of flexion, $\boldsymbol{CD}$, was the line connecting the two instant centers of curvature.

During the process of repositioning knee joint to a given flexion angle, axis of flexion and instant radii were varying constantly as the irregular shape of femoral condyle. At any instant, calculated axis of flexion was only valid for the corresponding contact point. Thus the entire adjustment process for flexion needed to be completed step by step. Within each iteration step tibia and attached components were rotated along instant axis of flexion with a pre-define increment which was small enough to converge a realistic knee joint motion.

Slight internal/external rotation and should be accounted for in modeling realistic knee joint motion. Axis of internal/external rotation is along the line connecting contact point at medial tibial plateau and ankle center (Figure 5). In walking posture, tibia presented internal rotation at most time.

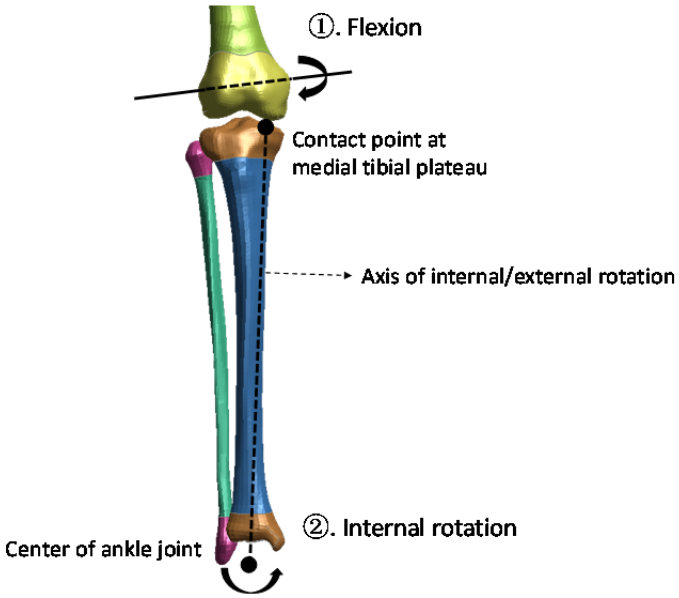

Fig. 5. Within each step in the iteration of flexion calculation, moving parts, including tibia and attached components, such as fibula, would be rotate along the axis of flexion. Subsequently, the moving parts would be conducted internal rotation along the axis connecting contact point on medial tibial plateau and center of ankle joint. During the calculated, direction of the axis of internal/external rotation needed to be updated along with flexion.

Compared with flexion, the angle of internal rotation was in a narrower range within a full gait cycle. In this study motion in this dimension were quantified by statistical results of experiments. Iwaki and Asano had presented history of averaged translational motion for contact points on tibial plateau for lateral side with or without vertical loading of upper body on the knee joint (Figure 6) [16][17]. Contact points were almost static on medial condyle based on experimental results (Figure 7), leading to the assumption that axis for internal rotation of tibia passed through contact point on medial condyle.

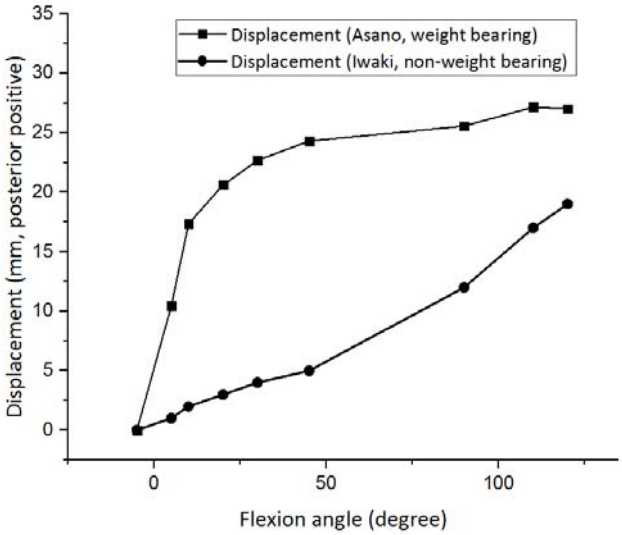

Fig. 6. Statistical data of displacement of lateral contact point on tibial condyle in Iwaki and Asano's study [16][17]

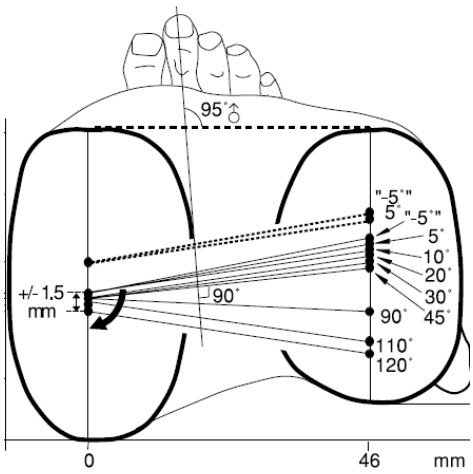

Fig. 7. Schematic of trace of lateral contact point. As tibial internal rotation happened, the contact point was moving posteriorly on the tibial plateau [16]

In Figure 6, knee joint with upper body load presented more obvious internal rotation with flexion. In normal gait cycle, a leg could be in "stance" (contacting the ground) or "swing" phase. The algorithm was able to judge state of the leg to determine which dataset (Iwaki's study – without upper body load, corresponding with "swing phase"; Asano's, on the contrary) would be chosen to quantify angle of internal/external rotation at the given instant.

In each step of iteration for knee joint adjustment, corresponding increment of internal rotation would be determined by iterations. When deviation of displacement of contact point on lateral tibial plateau from predicted value (Figure 6) is smaller than given threshold, the iteration terminates, and the increment would be assigned to rotation along the axis for tibia and attached structures (Figure 6).

Mesh morphing for the transitional parts

Mesh morphing method has been widely utilized to change size and shape of FE model, especially in the field of parametrical human body modeling. In this study, landmark-based Radial Basis Function (RBF) interpolation was used to morph the transition parts to adapt to the bone motions. To achieve this, landmarks were identified on the bone structures adjacent to the soft tissues. Coordinates of landmarks were determined based on bone motions before and after posture adjustment. RBF calculated the deformation field based on the landmarks and morphed the mesh of the surrounding soft tissues. Detailed introduction to RBF mesh morphing method was given in [18]. Application of mesh morphing method had been well documented in previous studies [19-22].

III. RESULTS

Validation of the algorithm

Since no realistic gaits of the subjects whose geometry was collected for GHBMC model are available, currently results predicted in this study cannot be validated against physical testing data. However, the lower extremity posture of the GHBMC pedestrian model was adjusted to replicate the posture of GHBMC occupant model, in which the subject was in a driving posture. Geometry of the two models were supposed to be collected from subjects of similar anthropometry in different postures. It was found that except for the shape of the menisci, the bone locations and the soft tissue shapes were similar between the re-positioned pedestrian model and the occupant model (Figure 8), indicating that the algorithm was effective in posture adjustment.

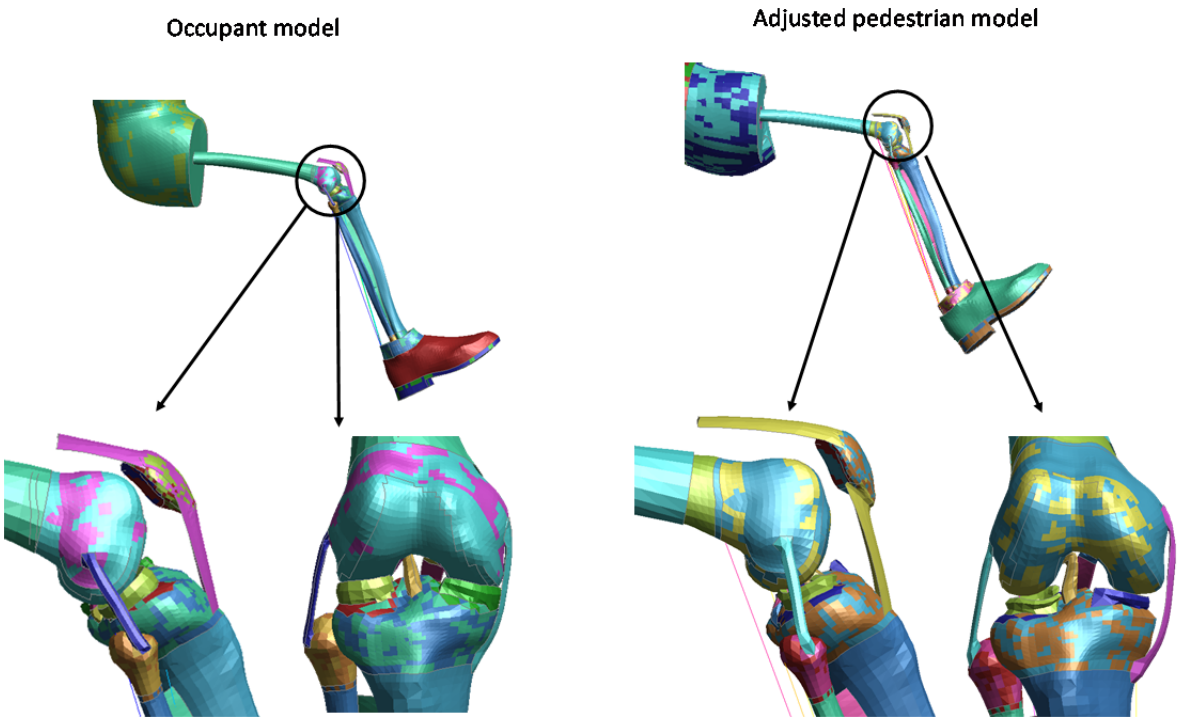

Fig. 8. Comparison in detailed of knee joint structures between GHBMC occupant model and pedestrian model adjusted to similar posture

Increments of 0.5 and 0.1 degree were defined respectively to investigate influence of the amount of increment for flexion angle on the predicted motion. The predicted instant radii indicated that 0.5 degree was small enough for the convergence of the results given the close results between the two (Figure 9).

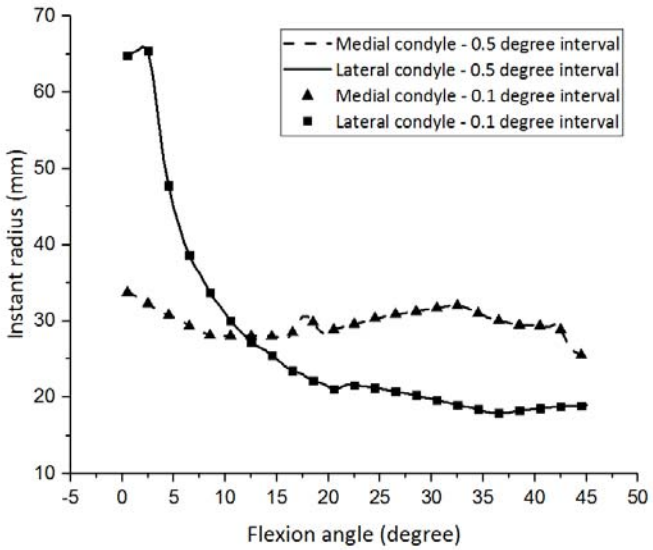

Fig. 9. Predicted instant radii on medial and lateral femoral condyles with increment of 0.1 and 0.5 degree for flexion angle

Pedestrian models with different postures

For a single posture adjustment, it took less than 40 minutes to implement the algorithm in MATLAB on a conventional PC, with the mesh quality remaining similar to the baseline model. Three pedestrian models with different walking postures in a gait cycle, i.e., heel contact, toe off and mid-swing stances, were generated (Figure 10). Mesh quality of the predicted models were at a comparable level with baseline (Table I).

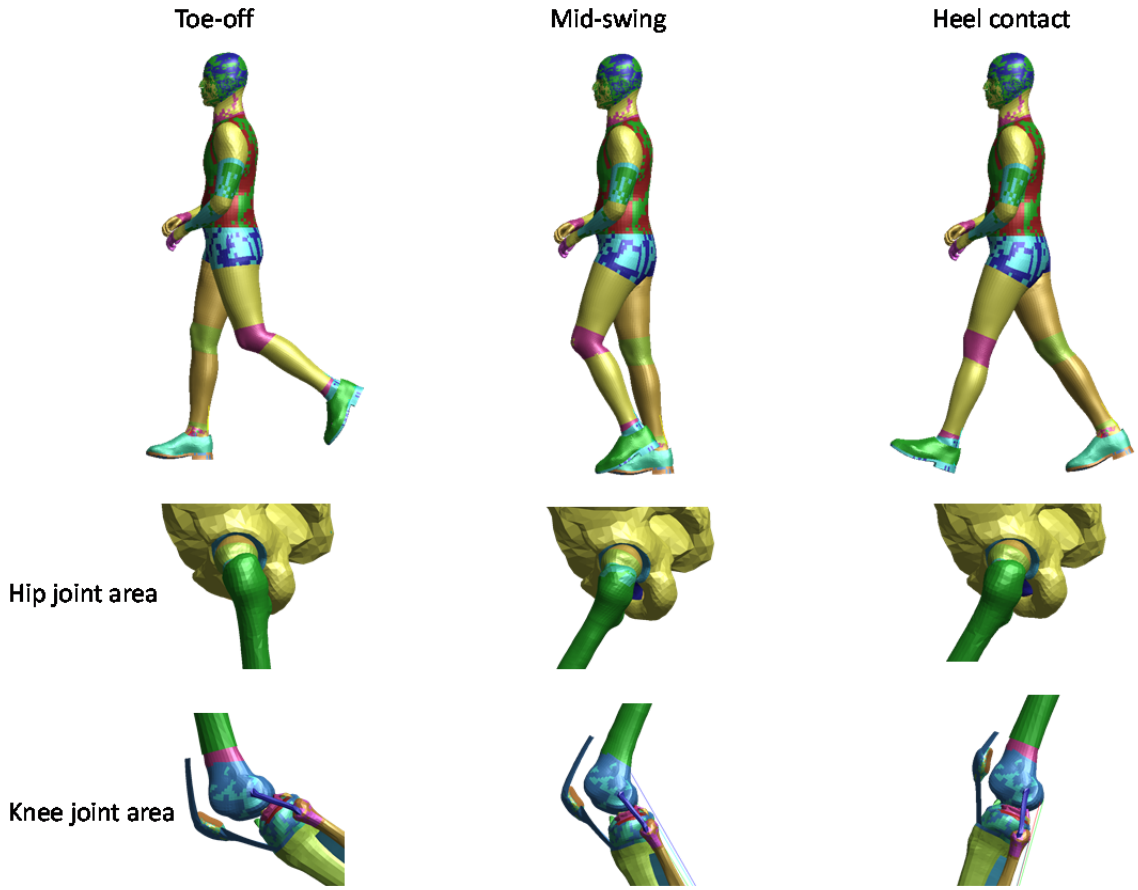

Fig. 10. Illustration of three model generated with different gaits – toe-off, mid-swing and heel contact in sequence for left leg. Details at hip joint and knee joint area of left leg were also depicted.

TABLE I
MESH QUALITY OF ADJUSTED MODELS COMPARING TO BASELINE

Model	Number of shell elements (Jacobian value <0.7, minimum value in bracket)	Number of solid elements (Jacobian value <0.3)
Baseline	3862 (2%, 0.40)	0 (0%, 0.3)
Toe-off	3865 (2%, 0.40)	5 (0%, 0.16)
Mid-swing	3870 (2%, 0.40)	2 (0%, 0.30)
Heel contact	3871 (2%, 0.40)	5 (0%, 0.18)

Pedestrian posture effects on impact responses

The three models were used to simulate a 30 kph vehicle-to-pedestrian crash scenario, in which the pedestrians were impacted from the lateral side. Kinematic responses are illustrated in Figure 11. Kinematics of the pedestrian was substantially influenced by the relative position between the two legs.

The injury outcomes of the pedestrians are summarized in Table II. Among the three walking postures, mid-swing case sustained the highest fibula plastic strain of 15.9% after impact, and in all cases plastic strain of long bones had exceeded threshold (3% plastic strain) indicating bone fracture might occur during the impact. Heel contact case exhibited the highest ACL principal stress of 45.07 MPa, higher than toe off case (35.67 MPa). Simulation results confirmed that pre-crash posture would affect injury risks. This indicated that pedestrian pre-crash posture needs to be considered when predicting pedestrian impact responses.

TABLE II
INJURY OUTCOMES OF PEDESTRIANS IN DIFFERENT GAITS

Model	Maximum plastic strain of long bones	Maximum principal stress in knee joint ligaments (MPa)
Toe-off	8.3%	35.67
Mid-swing	15.9%	38.78
Heel contact	11.3%	45.07

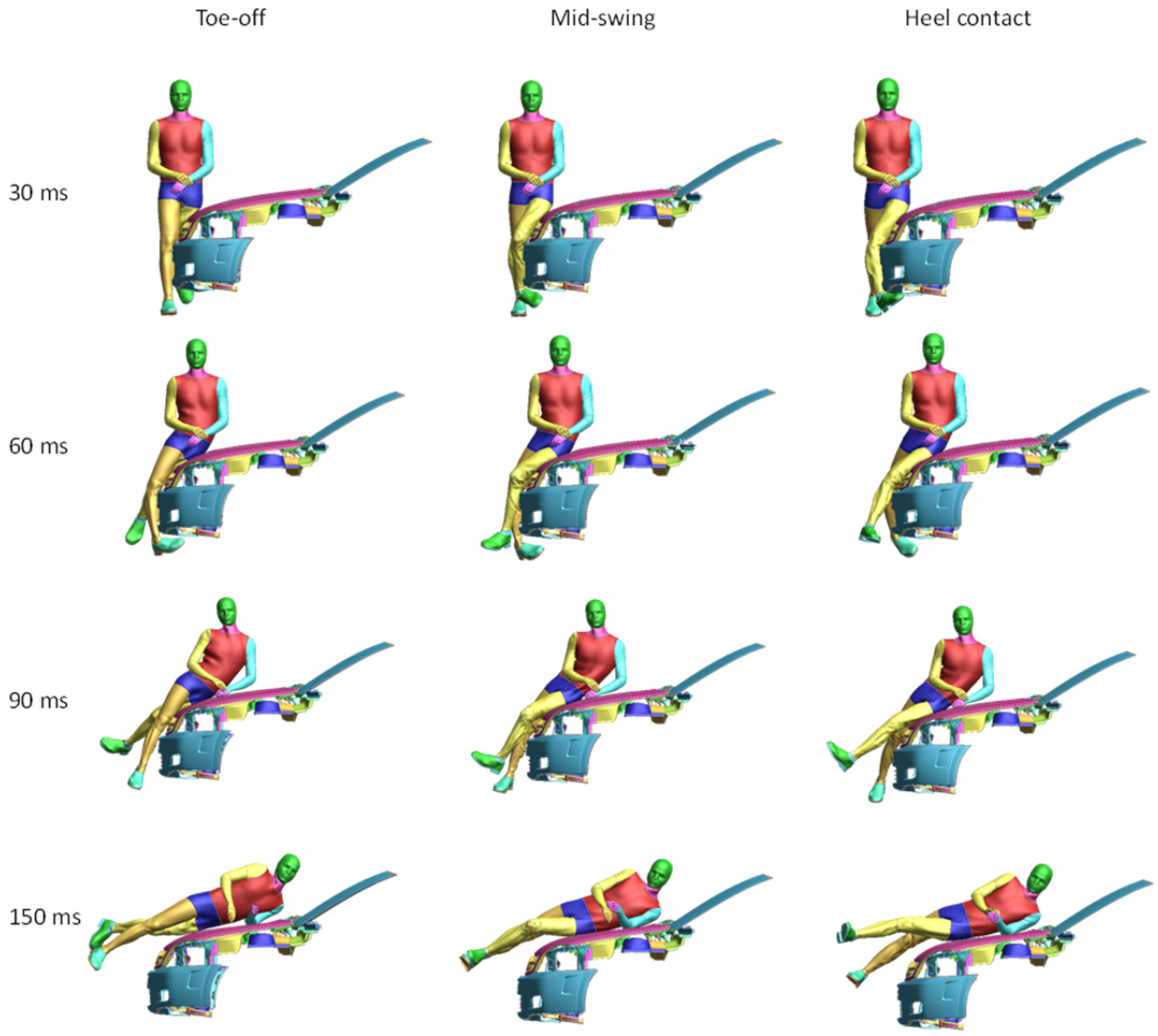

Fig. 11. Kinematics of pedestrian in different gaits impacted by vehicle front-end.

Instant radii at femoral condyles

For the knee joint, the proposed algorithm calculated the curvature and instant radii at the contact points during flexion. Instant radii vs. flexion angle curves are shown in Figure 12. In Iwaki's study, the instant radii for flexion facet of medial and lateral femoral condyles were approximated at 22 and 21 mm, respectively. The radii calculated in this study were close to the value provided above when flexion angle exceeds 20 degree. When the flexion angle is below 20 degree, instant radius at lateral condyle was almost 3 times as the statistical value. This may be attributed to the geometry of lateral femoral condyles of the GHBMC model. The inferior portion of the lateral condyle surface is flat, leading to a large instant radius. The shape of the posterior portion of the lateral condyle is more regular, and consequently similar value was predicted compared to the test data. These results indicated that the algorithm was able to consider detailed geometry of the source model.

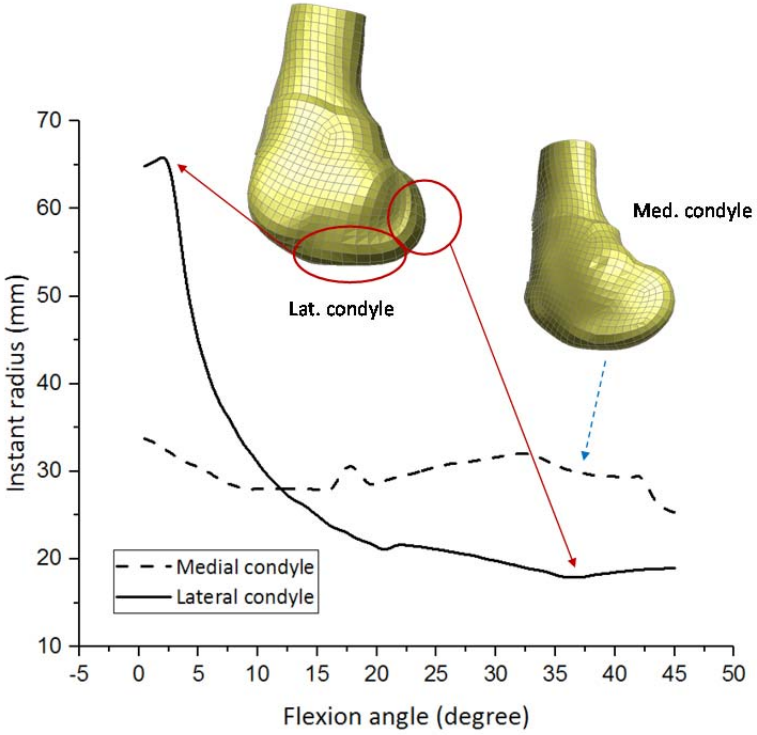

Fig. 12. Instant radii for medial and lateral femoral condyles vs. flexion angle

IV. DISCUSSION

This study presented a biomechanically realistic and computationally efficient algorithm to rapidly predict joint motion at a given gait considering realistic joint anatomy and kinematics. A framework has been established to do posture adjustment of an existing FE human body model. The process, in sequence, included dividing components into different categories based on kinematics, determining joint motion, and mesh morphing for the transitional parts. Specific geometry of the human body model were taken into account in estimating the joint kinematics, and algorithm in numerical surface reconstruction and calculation of instant radii were developed.

Complexity of the algorithm

Currently internal/external rotation of the tibia cannot be fully predicted based on the model geometry, and statistical data needs to be referred to. Future research efforts need to be devoted to improve the modeling of connective tissues to quantify the interaction of soft tissues and bones at the knee joint. The algorithm mainly focused on determination of flexion motion. To make the algorithm more integrated, internal rotation had been taken into consideration. Given the fact that tibial internal rotation angle was quite small compared to the flexion angle within a full gait cycle, prediction of Prediction of internal rotation could be removed to reduce complexity of the algorithm under the circumstances that influence of internal rotation is not significant in practice use.

Limitations

Local surface construction in the present algorithm was developed based on quadrilateral meshes and has not been expanded to the other element types (e.g. triangle) yet. It was operative for GHBMC model since meshes around femoral condyle area were in quadrilateral form. This issue needs be address when the algorithm being expanded to model with more general mesh.

Lagrangian interpolation was used as a preliminary approach for surface reconstruction, while more advanced surface reconstruction method, such as B-spline, can be incorporated to improve the precision and geometry quality.

Posture adjustment of upper torso and upper body was not included in current study. Thus the

corresponding parts were not adjusted in the generated model. Studies concerning these parts could be conducted based on the developed algorithm in the future.

Lacking of extensive validation against experimental data was also a limitation that has been explained in the section of results. To further validate the algorithm proposed in this study, more experiments on gait analysis need to be conducted with imaging technologies, and subject-specific human model simulations need to be conducted to reconstruct the testing conditions.

Potential application in future study

The presented work is applicable for a large set of human joints with similar geometrical structures and mechanism of joint motions. Therefore, the algorithm can be expanded to other moving joints in human body, such as shoulder, elbow and wrist joints, and can be applied for human model re-positioning beyond pedestrian.

The algorithm could also be implemented to generate a series of models with different gaits to investigate influence of pre-crash posture on pedestrian response in detail in future study.

V. CONCLUSIONS

A rapid posture adjustment algorithm for pedestrian lower extremities was developed to account for the realistic joint kinematics during a gait cycle. Under the kinematic constraints from joint anatomy, the algorithm calculated the posture of the lower extremities at any instant of a gait cycle from the open kinematic chain linked by the hip, knee and ankle joints in sequence. The algorithm calculated joint kinematics in knee flexion based on geometry reconstructed from subject-specific anatomical features. Mesh morphing method were implemented to calculate nodal coordinates of the transitional soft tissues.

Based on 50th percentile male GHBMC pedestrian model, three pedestrian models with different walking postures within a gait cycle were generated. These models were used to simulate a 30 kph vehicle-to-pedestrian crash scenario and predicted injury outcomes were analyzed. Pre-crash posture showed significant effect on the injury risks of lower extremities in vehicle-to-pedestrian crashes.

VI. ACKNOWLEDGEMENT

The authors wish to thank Elemance, Altair, Arup and LSTC for providing academic license of GHBMC models, Hyperworks, Oasys and LS-DYNA software respectively.

VII. REFERENCES

[1] Organization, W.H. Global status report on road safety: time for action. Geneva. 2009. 2009, ISBN 978-92-4-156384-0. Department of Violence & Injury Prevention & Disability (VIP). Retrieve from http://whqlibdoc. who. int/publications/2009/9789241563840_eng. pdf.

[2] Yang, J. Review of injury biomechanics in car-pedestrian collisions. *International journal of vehicle safety*, 2005. 1(1-3): p. 100-117.

[3] Chidester, A.B. and Isenberg, R.A., "Final report: The pedestrian crash data study". 2001: Society of Automotive Engineers.

[4] Yang, J., Ries, O., Schoenpflug, M., and Brianso, C. Pedestrian position definition. *Deliverable D8, HUMOS2 Project, GRD-2001-50053*, 2003.

[5] Elliott, J., Simms, C., and Wood, D.P. Pedestrian head translation, rotation and impact velocity: The influence of vehicle speed, pedestrian speed and pedestrian gait. *Accident Analysis & Prevention*, 2012. 45: p. 342-353.

[6] Peng, Y., Deck, C., Yang, J., and Willinger, R. Effects of pedestrian gait, vehicle-front geometry and impact velocity on kinematics of adult and child pedestrian head. *International Journal of Crashworthiness*, 2012. 17(5): p. 553-561.

[7] Untaroiu, C.D., Meissner, M.U., et al. Crash reconstruction of pedestrian accidents using optimization techniques. *International Journal of Impact Engineering*, 2009. 36(2): p. 210-219.

[8] Li, G., Yang, J., and Simms, C. Predicting the effects of pedestrian gait on lower limb injuries. *Proceedings of IRCOBI Conference Proceedings*, 2014.

[9] Tang, J., Zhou, Q., Nie, B., Yasuki, T., and Kitagawa, Y. Influence of Pre-impact Pedestrian Posture on Lower Extremity Kinematics in Vehicle Collisions. *SAE International Journal of Transportation Safety*, 2016. 4(2016-01-1507): p. 278-288.
[10]Jani, D., Chawla, A., et al. Repositioning the knee joint in human body FE models using a graphics-based technique. *Traffic injury prevention*, 2012. 13(6): p. 640-649.
[11]Levine, D., Richards, J., and Whittle, M.W., "Whittle's gait analysis". 2012: Elsevier Health Sciences.
[12]Grood, Edward S., and Wilfredo J. Suntay. A joint coordinate system for the clinical description of three-dimensional motions: application to the knee. *Journal of biomechanical engineering*, 1983.105(2): p. 136-144.
[13]Adouni, M., A. Shirazi-Adl, and R. Shirazi. Computational biodynamics of human knee joint in gait: from muscle forces to cartilage stresses. *Journal of biomechanics*, 2012.45(12): p. 2149-2156.
[14]Zachman, N. J., B. M. Hillberry, and D. B. Kettelkamp. Design of a load simulator for the dynamic evaluation of prosthetic knee joints. *American Society of Mechanical Engineerers*, 1978.
[15]Halloran, Jason P., Anthony J. Petrella, and Paul J. Rullkoetter. Explicit finite element modeling of total knee replacement mechanics. *Journal of biomechanics*, 2005. 38(2): p. 323-331.
[16]Iwaki, H., Pinskerova, V., and Freeman, M. Tibiofemoral movement 1: the shapes and relative movements of the femur and tibia in the unloaded cadaver knee. *Bone & Joint Journal*, 2000. 82(8): p. 1189-1195.
[17]Asano, T., Akagi, M., Tanaka, K., Tamura, J., and Nakamura, T. In vivo three-dimensional knee kinematics using a biplanar image-matching technique. *Clinical Orthopaedics and Related Research*, 2001. 388: p. 157-166.
[18]Hwang, E., Hallman, J., et al. Rapid Development of Diverse Human Body Models for Crash Simulations through Mesh Morphing. 2016, SAE Technical Paper.
[19]Jingwen, H., Rupp, J.D., and Reed, M.P. Focusing on vulnerable populations in crashes: recent advances in finite element human models for injury biomechanics research. *J. Automot. Saf. Energy*, 2012. 3: p. 295-307.
[20]Li, Z., Hu, J., et al. Development, validation, and application of a parametric pediatric head finite element model for impact simulations. *Annals of biomedical engineering*, 2011. 39(12): p. 2984-2997.
[21]Li, Z., Hu, J., and Zhang, J. Comparison of different radial basis functions in developing subject-specific infant head finite element models for injury biomechanics study. *Proceedings of ASME 2012 Summer Bioengineering Conference*, 2012.
[22]Shi, X., Cao, L., Reed, M.P., Rupp, J.D., and Hu, J. Effects of obesity on occupant responses in frontal crashes: a simulation analysis using human body models. *Computer methods in biomechanics and biomedical engineering*, 2015. 18(12): p. 1280-1292.

VIII. APPENDIX

Appendix A

To rotate a vector by angle θ along a given axis passing the origin, expressed as $v=(v_1,v_2,v_3)$ in three dimensions, the rotation matrix R could be constructed based on given parameters, as depicted below.

$$R=\begin{bmatrix} \cos\theta+v_1^2(1-\cos\theta) & v_1v_2(1-\cos\theta)-v_3\sin\theta & v_1v_3(1-\cos\theta)+v_2\sin\theta \\ v_1v_2(1-\cos\theta)+v_3\sin\theta & \cos\theta+v_2^2(1-\cos\theta) & v_2v_3(1-\cos\theta)-v_1\sin\theta \\ v_1v_3(1-\cos\theta)-v_2\sin\theta & v_2v_3(1-\cos\theta)+v_1\sin\theta & \cos\theta+v_3^2(1-\cos\theta) \end{bmatrix}, \quad (4)$$

Appendix B

To reconstruction local surface around the contact points at femoral condyles, 9 elements in a 3×3 matrix were recruited (Figure 13). Corresponding contact points lied in the middle of the matrix.

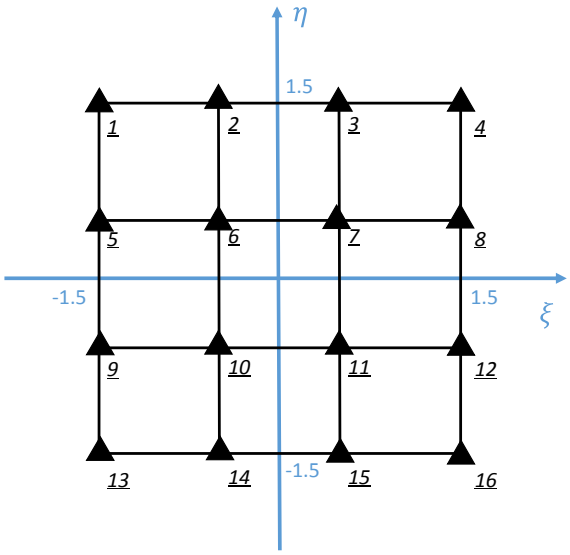

Fig. 13. Schematic of local surface reconstruction

To establish analytical expression, the surface were parameterized by two parameters – ξ and η, constructing a two-dimensional natural coordinates. As elements on femoral condyle surface were quadrilateral elements, there were totally 16 nodes within the matrix. All the nodes were aligned in sequence and been assigned a unique natural coordinate respectively.

Lagrangian interpolation were implemented in surface reconstruction. For a mesh with m+1 rows and n+1 columns, the interpolation function N_i of node i positioned at the intersection of row I and column J could be written as

$$l_I^{\,m}(\xi)=\frac{(\xi-\xi_1)(\xi-\xi_2)\cdots(\xi-\xi_{I-1})(\xi-\xi_{I+1})\cdots(\xi-\xi_n)}{(\xi_J-\xi_1)(\xi_J-\xi_2)\cdots(\xi_I-\xi_{I-1})(\xi_I-\xi_{I+1})\cdots(\xi_J-\xi_n)}, \tag{5}$$

$$l_J^{\,n}(\eta)=\frac{(\eta-\eta_1)(\eta-\eta_2)\cdots(\eta-\eta_{J-1})(\eta-\eta_{J+1})\cdots(\eta-\eta_n)}{(\eta_J-\eta_1)(\eta_J-\eta_2)\cdots(\eta_J-\eta_{J-1})(\eta_J-\eta_{J+1})\cdots(\eta_J-\eta_n)}, \tag{6}$$

$$N_i=N_{IJ}=l_I^{\,m}(\xi)\cdot l_J^{\,n}(\eta), \tag{7}$$

In current study, I=3, J=3, and take i = 1,9,16 for examples,

$$N_1=-((-8\xi^3+12\xi^2+2\xi-3)\cdot(-8\eta^3-12\eta^2+2\eta+3))/2304, \tag{8}$$

$$N_9=-((-8\xi^3+12\xi^2+2\xi-3)\cdot(-8\eta^3+4\eta^2+18\eta-9))/768, \tag{9}$$

$$N_{16}=-((-8\xi^3-12\xi^2+2\xi+3)\cdot(-8\eta^3+12\eta^2+2\eta-3))/2304, \tag{10}$$

For points with coordinate (ξ^*,η^*) in the natural coordinates, corresponding coordinate in global Cartesian coordinates of the FE model would be interpolated as

$$x(\xi^*,\eta^*)=\sum_{i=1}^{16}N_i(\xi^*,\eta^*)x_i, \tag{11}$$

$$y(\xi^*,\eta^*)=\sum_{i=1}^{16}N_i(\xi^*,\eta^*)y_i, \tag{12}$$

$$z(\xi^*,\eta^*)=\sum_{i=1}^{16}N_i(\xi^*,\eta^*)z_i,$$

(13)

Appendix C

There were 2 covariant vectors, which also could be regarded as base vectors for tangent plane at contact point, as shown in equation (4) and (5).

$$\boldsymbol{g}_1 = \boldsymbol{g}_\xi = \frac{\partial \boldsymbol{x}}{\partial \xi} = \left(\frac{\partial\left(\sum_{i=1}^{16} N_i x_i\right)}{\partial \xi}, \frac{\partial\left(\sum_{i=1}^{16} N_i y_i\right)}{\partial \xi}, \frac{\partial\left(\sum_{i=1}^{16} N_i Z_i\right)}{\partial \xi} \right),$$

(14)

$$\boldsymbol{g}_2 = \boldsymbol{g}_\eta = \frac{\partial \boldsymbol{x}}{\partial \eta} = \left(\frac{\partial\left(\sum_{i=1}^{16} N_i x_i\right)}{\partial \eta}, \frac{\partial\left(\sum_{i=1}^{16} N_i y_i\right)}{\partial \eta}, \frac{\partial\left(\sum_{i=1}^{16} N_i Z_i\right)}{\partial \eta} \right),$$

(15)

Normal vector is cross production of the tangent vectors. Calculation of unit normal vector was expressed as (6).

$$\boldsymbol{n} = \frac{\boldsymbol{g}_1 \times \boldsymbol{g}_2}{\left|\boldsymbol{g}_1 \times \boldsymbol{g}_2\right|}, \tag{16}$$

With the element of arc on the surface being expressed as

$$\boldsymbol{ds} = d\zeta^\alpha \boldsymbol{g}_\alpha, \tag{17}$$

The first fundamental form I represented length of element of arc.

$$I = ds^2 = d\zeta^\alpha \boldsymbol{g}_\alpha \cdot d\zeta^\beta \boldsymbol{g}_\beta = a_{\alpha\beta} d\zeta^\alpha d\zeta^\beta, \tag{18}$$

Where

$$a_{\alpha\beta} = \boldsymbol{g}_\alpha \cdot \boldsymbol{g}_\beta,$$

(19)

The second fundamental form II could be calculated by

$$II = b_{\alpha\beta} d\zeta^\alpha d\zeta^\beta = \boldsymbol{n} \cdot \frac{\partial^2 \boldsymbol{\rho}}{\partial \zeta^\alpha \partial \zeta^\beta} d\zeta^\alpha d\zeta^\beta = \boldsymbol{n} \cdot \frac{\partial^2 \boldsymbol{g}_\alpha}{\partial \zeta^\beta} d\zeta^\alpha d\zeta^\beta = -\frac{\partial \boldsymbol{n}}{\partial \zeta^\beta} \cdot \boldsymbol{g}_\alpha d\zeta^\alpha d\zeta^\beta ,$$

(20)